JOURNAL OF SOLID STATE CHEMISTRY 66, 105–115 (1987)

Further Aspects of the Structure and Magnetism of the Layered Compound Fe(III)ClMoO$_4$: Mössbauer Spectroscopy, Susceptibility, and Powder Neutron Diffraction Studies

C. C. TORARDI

E. I. du Pont de Nemours & Company, Central Research and Development Department,[1] *Experimental Station, Wilmington, Delaware 19898*

W. M. REIFF, K. LÁZÁR, AND J. H. ZHANG

Department of Chemistry, Northeastern University, Boston, Massachusetts 02115

AND D. E. COX

Brookhaven National Laboratory, Department of Physics, Upton, Long Island, New York 11973

Received December 30, 1985; in revised form April 28, 1986

Aspects of the nuclear and magnetic structure of the three-dimensionally ordered state of the layered system Fe(III)ClMoO$_4$ are elucidated primarily on the basis of single crystal and powder Mössbauer spectroscopy and neutron powder diffraction refinements at various temperatures. The antiferromagnetically coupled spins and easy axis of magnetization for Fe(III)ClMoO$_4$ are indicated to lie in the tetragonal layers (*ab* planes) perpendicular to the *c* axis, which is parallel to the Fe–Cl bond vector of a local C_{4v} FeO$_4$Cl chromophore. Additionally, the neutron diffraction data indicate a very significant *c*-axis contraction with decreasing temperature (2.7% between 295 and 5 K), with the rate of contraction being highest in the vicinity of the Néel temperature, T_N (~70 K). The structural changes that occur in the temperature range 300 to 5 K are discussed. Powder and single crystal magnetic susceptibility results to ~1.6 K as well as high field Mössbauer spectra to ~9 T are also presented. The latter indicate a spin flop transition with H_{sf} ~1 T. Alternate views of the low-dimensional magnetism of FeClMoO$_4$, evident as a broad maximum in its molar susceptibility at ~105 K, are discussed.

Introduction

In a recent investigation, we reported the synthesis, X-ray structure determination, and features of the low-temperature magnetic properties of the new compound Fe(III)ClMoO$_4$ (*1*). This material crystallizes with tetragonal symmetry (a = 6.672(3) and c = 5.223(3) Å) in space group $P4/nmm$ with Z = 2. A view along the c axis showing two FeClMoO$_4$ sheets, each composed of corner-shared FeO$_4$Cl square pyramids and MoO$_4$ tetrahedra, is given in Fig. 1. A powdered sample exhibits a well-

[1] Contribution No. 3881.

0022-4596/87 $3.00

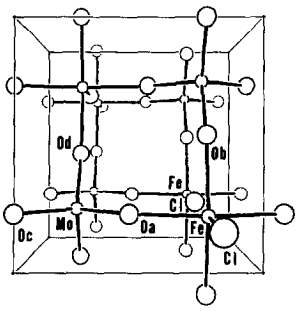

FIG. 1. A view along the c axis of $FeClMoO_4$ and perpendicular to two stacked layers, each composed of corner-sharing MoO_4 tetrahedra and FeO_4Cl square pyramids.

defined but broad maximum in the temperature dependence of its molar susceptibility (χ'_m) centered at ~105 K signaling some type of low-dimensional magnetic behavior. Zero field Mössbauer spectra (*1*) for polycrystalline powder samples show magnetic hyperfine splitting ($H_{Internal}$ (0° K) ≈482 kG) and indicate three-dimensional ordering, $T_N = 69.2$ K. In the present work, single crystal susceptibility and Mössbauer spectroscopy results as well as powder neutron diffraction and high field Mössbauer data are presented in an attempt to further clarify the nature of the low- and three-dimensional magnetic properties of $Fe(III)ClMoO_4$.

Experimental

1. Magnetic Susceptibility and Mössbauer Measurements

Crystalline plates of tetragonal $FeClMoO_4$ with dimensions as large as 8 mm across the plate and 3 mm thick were grown as described previously (*1*). Powder magnetic susceptibility data and zero field Mössbauer spectra were determined as reported earlier (*2*). High field Mössbauer spectra were determined using a niobium–titanium solenoid capable of applied fields, H_o, up to 9 T. The geometry was longitudinal ($H_o \| \bar{E}_\gamma$) with the source always maintained in the central field (H_o at the source ≤ 0.1 T) of an opposing "buck out coil" so as to minimize broadening effects from the fringe field of the primary solenoid. Due to the layered structure of $FeClMoO_4$, crystals were easily cleaved to obtain *ab* slices. The single crystal spectra were determined for a mosaic of thin (~0.5 mm thick) sections oriented such that the c axis was parallel to $\bar{E}_\gamma$ and H_o. This was the only orientation that could be conveniently obtained which at the same time did not present undue mass attenuation of the gamma ray beam. Single crystal magnetic susceptibility measurements were made using the SQUID facilities available at the Francis Bitter National Magnet Laboratory.

2. Neutron Powder Diffraction

Neutron diffraction scans were carried out at the Brookhaven National Laboratory High-Flux Beam Reactor. For these experiments, a powdered sample was loaded into a cylindrical aluminum holder about 1 cm in diameter under an atmosphere of dry helium. Full sets of data suitable for Rietveld refinement were collected at 4.85, 70, and 181 K. In addition, a few scans were made at intermediate temperatures to check the magnetic intensities and the lattice constants. The experimental configuration consisted of a pyrolytic graphite monochromator and analyzer in the (002) setting. Collimation was set at 20′, 40′, 40′, and 20′, respectively, for the in-pile, monochromator-sample, sample-analyzer, and analyzer-detector locations. The neutron wavelength was 2.382 Å, and higher order components were suppressed with a graphite filter.

The neutron diffraction data for $FeClMoO_4$ at 70 and 181 K were fitted by refinement of the structure in space group $P4/nmm$ (No. 129) using the Rietveld profile method (*3*). Atomic positions from the room temperature single crystal X-ray structural refinement (*1*) were used for the

TABLE I

PARAMETERS FROM RIETVELD AND SINGLE CRYSTAL X-RAY REFINEMENTS OF FeClMoO$_4$

Parameter	T = 4.85 K	T = 70 K	T = 181 K	T = 300 K[a]
Mo, x	0.75	0.75	0.75	0.75
y	0.25	0.25	0.25	0.25
z	0.00	0.00	0.00	0.00
B (Å^2)	0.5(1)	0.5(1)	0.9(1)	0.8
Fe, x	0.25	0.25	0.25	0.25
y	0.25	0.25	0.25	0.25
z	0.2704(8)	0.2713(7)	0.2736(7)	0.2728(1)
B (Å^2)	1.1(1)	0.1(1)	0.3(1)	0.8
Moment (μ_B)	4.21(3)			
Cl, x	0.25	0.25	0.25	0.25
y	0.25	0.25	0.25	0.25
z	0.7091(8)	0.7060(7)	0.6993(8)	0.6956(2)
B (Å^2)	0.5(1)	0.5(1)	1.2(1)	2.3
O, x	0.25	0.25	0.25	0.25
y	0.9608(4)	0.9620(4)	0.9630(4)	0.9633(2)
z	0.2067(6)	0.2026(6)	0.1998(6)	0.1968(3)
B (Å^2)	0.6(1)	0.6(1)	0.9(1)	1.6
G	0.116(5)	0.109(5)	0.095(5)	—
a (Å)	6.6849(2)	6.6828(2)	6.6680(2)	6.6694(4)
c (Å)	5.0887(3)	5.1259(2)	5.1914(3)	5.228(1)
R_N (%)	5.4	5.5	4.9	
R_{WP} (%)	9.2	9.7	9.2	
R_M (%)	7.3	—	—	
R_E (%)	3.5	4.7	4.8	

[a] Single crystal X-ray structure, Ref. (*1*).

initial values, and individual isotropic temperature factors were refined. Regions of the scan which included the diffraction peaks of the aluminum sample container were excluded from the refinement. Other variables included in the structural refinement were half-width parameters, zero point, cell constants, and in the later stages of refinement a uniaxial preferred orientation parameter of the type suggested by Rietveld. Neutron cross sections were taken from Koester (*4*). Convergence was quickly reached, and the final positional, thermal, preferred orientation, and lattice parameters are listed in Table I together with the X-ray values. The overall agreement is very good with weighted profile R-factors, R_{WP}, close to the expected or statistical values, R_E.

Below the three-dimensional antiferromagnetic ordering temperature, $T_N \approx 70$ K, magnetic scattering peaks appear in the diffraction patterns. These peaks are commensurate with a larger cell and can be indexed by doubling the a and c tetragonal lattice parameters; with h, k, and l all odd. This means that each of the two moments in the chemical cell must be coupled antiparallel to its neighbors in adjacent unit cells separated by a or c, and it only remains to determine the relative orientation of the two moments at $\pm\frac{1}{4}\ \frac{1}{4}\ z$ (i.e., $\pm\frac{1}{8}\ \frac{1}{8}\ z/2$ in the magnetic cell). Inspection of the magnetic intensities showed that the moments must be in or close to the basal plane, and therefore *noncollinear models with tetragonal symmetry should be considered as well as collinear models*. Intensity calculations were made for the first four magnetic peaks for a number of models with the two moments parallel, antiparallel, or at 90° to each other, and directed along the ⟨100⟩ or ⟨110⟩ axes (Table II). As is often the case in powder magnetic studies, there is some degeneracy, and it turns out that the models can be grouped into three intensity sets, as shown in Table II.

The noncollinear models have tetragonal symmetry (point groups $\bar{4}2m$ or $\bar{4}$ depending on the moment direction) and the collinear models have either orthorhombic (mmm) or monoclinic ($2/m$) symmetry. The

TABLE II

CLASSIFICATION OF MAGNETIC MODELS INTO THREE INTENSITY GROUPS, AS DISCUSSED IN TEXT FOR FeClMoO$_4$; S_1 AND S_2 REPRESENT MOMENTS AT $\frac{1}{8}\ \frac{1}{8}\ z$ AND $\bar{\frac{1}{8}}\ \bar{\frac{1}{8}}\ \bar{z}$, RESPECTIVELY

	I	II	III			
	Tetragonal ($\bar{4}2m$)	Tetragonal ($\bar{4}2m$)	Tetragonal ($\bar{4}$)			
S_1	[100]	[010]	[100]	[010]	[110]	[110]	[1$\bar{1}$0]	[1$\bar{1}$0]
S_2	[010]	[100]	[0$\bar{1}$0]	[$\bar{1}$00]	[1$\bar{1}$0]	[110]	[110]	[1$\bar{1}$0]
	Othorhombic (mmm)	Othorhombic (mmm)	Monoclinic ($2/m$)			
S_1	[110]	[1$\bar{1}$0]	[110]	[1$\bar{1}$0]	[100]	[010]	[$\bar{1}$00]	[0$\bar{1}$0]
S_2	[110]	[$\bar{1}$10]	[1$\bar{1}$0]	[$\bar{1}$10]	[100]	[010]	[$\bar{1}$00]	[0$\bar{1}$0]

TABLE III

COMPARISON OF OBSERVED AND CALCULATED INTENSITIES FOR $FeClMoO_4$ NORMALIZED TO $I(\frac{1}{2}\frac{1}{2}\frac{1}{2})$ FOR MODELS IN INTENSITY GROUPS I, II, AND III AS SUMMARIZED IN TABLE II

	I (calcd)			I (obs)
hkl	I	II	III	
$\frac{1}{2}\frac{1}{2}\frac{1}{2}$	1.00	1.00	1.00	1.00
$\frac{3}{2}\frac{1}{2}\frac{1}{2}$	0.48	0.39	0.43	0.36
$\frac{1}{2}\frac{1}{2}\frac{3}{2}$	0.23	0.20	0.22	0.18
$\frac{3}{2}\frac{3}{2}\frac{1}{2}$	0.10	0.11	0.11	0.11
R_N	5.2	5.1	5.1	—
R_M	13.5	7.3	10.0	—
R_{WP}	9.9	9.2	9.4	—
R_E	3.5	3.5	3.5	—

Note. Values of I (obs) have been corrected for preferred orientation by a factor $\exp(-G\alpha^2)$, where G = 0.115 and α is the angle (in radians) between the scattering vector and [001]. The R-factors obtained from Rietveld refinement of one model in each group are given above.

three sets of calculated intensities, normalized to the strongest peak, $\frac{1}{2}\frac{1}{2}\frac{1}{2}$, are shown in Table III, together with the observed intensities corrected for preferred orientation. Agreement is clearly better for the models in group II and this is unequivocally confirmed by Rietveld refinement of a tetragonal model from each set, as shown by the respective R-factors (Table III). Atomic scattering factors for iron were taken from Watson and Freeman (*5*). Final refinement parameters are given in Table I.

Thus, two structures give an equally good fit to the data, one noncollinear, with magnetic space group $P_I\bar{4}m2$ and one collinear with space group $C_Imm'a$ (for notation see Opechowski and Guccione (*6*)). Neither of these permits a magnetic component along the [001] axis, and this was in fact confirmed by refinement of a component in this direction which resulted in a slightly higher R-factor and a value within one-half of a standard deviation from zero, $0.4 \pm 1.0\ \mu_B$.

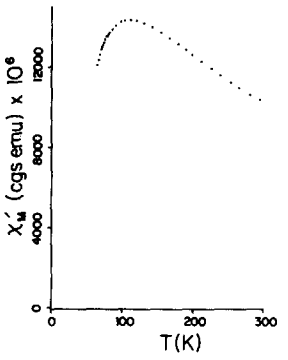

FIG. 2. The temperature dependence of the corrected molar susceptibility for $FeClMoO_4$ (powder) in the temperature range 300–50 K with H_0 = 5.1 kG.

Results and Discussion

1. Magnetic Susceptibility

The susceptibility results that we now describe prove to be inconclusive in forming a more complete picture of the low-temperature magnetic behavior of Fe(III)$ClMoO_4$. The original powder susceptibility data (*1*) determined over the range 300–50 K (Fig. 2) shows the broad maximum in χ'_m at ~105 K alluded to previously. We have extended these powder measurements to ~1.6 K in the present work as shown in Fig. 3. While the magnetic moment steadily decreases, the average power susceptibility begins to rise below ca. 40 K, an effect that we attribute to impurities. A few percent of impurity is suggested by zero field Mössbauer spectra to be discussed subsequently.

It was hoped that single crystal susceptibility measurements would be more informative than the powder results and that at the minimum, they would clearly indicate the direction of the easy axis of magnetization. For a uniaxial easy-axis antiferromagnet, $\chi_\perp$ should level off, becoming essentially constant with decreasing T for $T < T_N$, while $\chi_\parallel$ should approach zero with $\langle\chi\rangle_{powder} = \frac{1}{3}\chi_\parallel + \frac{2}{3}\chi_\perp$ (*7*). The results shown in Fig. 4 were obtained for large (~10–25 mg) opaque crystals. Unfortunately both sus-

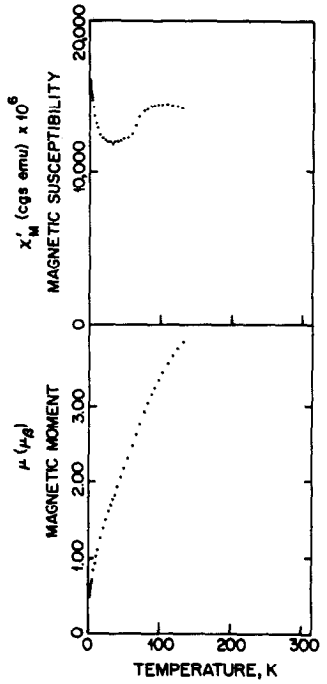

FIG. 3. Corrected molar susceptibility (top) and magnetic moment (bottom) for FeClMoO$_4$ (powder) in the temperature range 140–1.6 K.

ceptibilities tend to diverge at low temperature, again suggesting impurity effects and making an assignment of the easy axis ambiguous. One is tempted to assume that the c axis is easy as χ_m shows a small decrease below ~70 K (T_N) before rising at even lower temperatures. However, this assignment is at variance with Mössbauer spectroscopy and neutron diffraction data that we now discuss.

2. *Mössbauer Spectroscopy*

As mentioned in the introduction, the zero field quadrupole doublet spectrum of the paramagnetic phase undergoes hyperfine splitting suggesting three-dimensional ordering between 69 and 70 K. The fully resolved, low-temperature powder spectra (below T_N) clearly show the combined effects of magnetic hyperfine splitting with quadrupole perturbation in terms of a shift

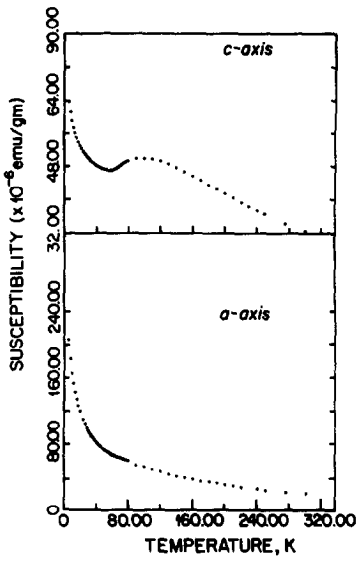

FIG. 4. Single crystal magnetic susceptibility of FeClMoO$_4$, H_0 along the a and c axes.

of the *center* of the inner four Zeeman transitions relative to that of the outer two (see Fig. 5, T = 52.8 K). The differential shift (S_1 − S_2), where S_1 is the separation of transitions one and two and S_2 is the separation

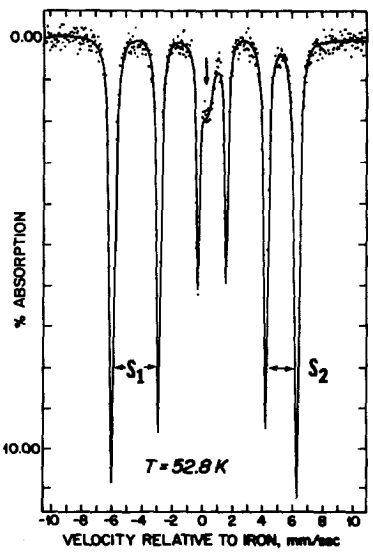

FIG. 5. Hyperfine split Mössbauer spectrum of FeClMoO$_4$ (powder) at $T < T_{Néel}$.

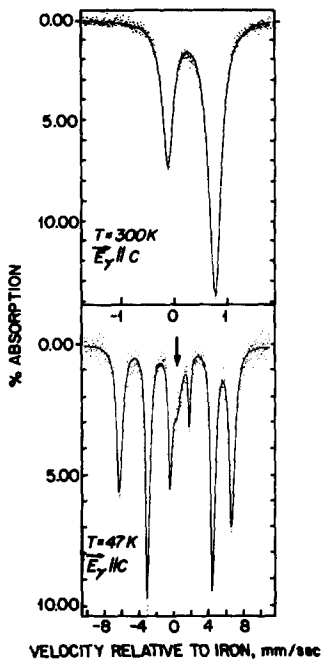

FIG. 6. Single crystal Mössbauer spectra for $FeClMoO_4$ above and below $T_{Néel}$ with the c axis parallel to $\vec{E}_\gamma$.

of transitions five and six, is positive. Its value remains essentially constant near unity and indicates the absence of any "Morin"-type behavior below T_N. For the case of an axially symmetric electric field gradient tensor, the differential shift is related to the quadrupole splitting of the *paramagnetic phase*, ΔE, by the relation: $S_1 - S_2 = -\Delta E\,(3\cos^2\theta - 1)$ where θ is the angle between the principal component of the electrical field gradient tensor, V_{zz}, and the internal hyperfine field (*8*). The foregoing equation has two possible solutions for θ when $S_1 - S_2 \leq \Delta E$, as in the present case. These correspond to $V_{zz} > 0$ and $V_{zz} < 0$. In view of the known structure, V_{zz} is most probably positive and coincidental with the short Fe–Cl bond. The basis for assuming that V_{zz} is positive is a simple point charge calculation for a near regular square pyramidal array of hard ligands and the fact that there is no valence shell orbital occupation contribution to the electrical field gradient for the half-filled (high spin) ferric shell (*9*). The solution for $V_{zz} > 0$ is $\theta = 90°$. That V_{zz} is in fact positive is confirmed by single crystal Mössbauer spectra at $T > T_N$, e.g., ambient temperature (Fig. 6) such that the direction of γ-ray propagation ($\vec{E}_\gamma$) is along the tetragonal c axis and normal to the $FeClMoO_4$ (ab) layers. The angular component of the probability function for $|\frac{1}{2}, \pm\frac{1}{2}\rangle \rightarrow |\frac{3}{2}, \pm\frac{1}{2}\rangle$ (σ γ-ray transitions) is $2 + 3\sin^2\theta$ while that for $|\frac{1}{2}, \pm\frac{1}{2}\rangle \rightarrow |\frac{3}{2}, \pm\frac{3}{2}\rangle$ (π γ-ray transition) is $3(1 + \cos^2\theta)$ where $E_\sigma < E_\pi$ corresponds to $V_{zz} > 0$ and θ is the angle between V_{zz} and $\vec{E}_\gamma$ (*8*). Under the foregoing experimental conditions, for a mosaic of single crystals, it was found that the intensity ratio, $I_-/I_+ = 0.45$ versus a theoretical value of $\frac{1}{3}$ for thin, perfectly oriented crystals. This is consistent with V_{zz} parallel to c (i.e., V_{zz} coincides with the Fe–Cl bond vector) and is *positive*. For $T < T_N$, single crystal spectra (Fig. 6) with the same orientation, ($\vec{E}_\gamma \| c$), show a pattern with substantial *enhancement of the intensities of the* $\Delta M_I = 0$ *transitions* (*transitions 2 and 5*) where θ is now the angle between $\vec{E}_\gamma$ and H_{int}. The angular components of the selection rules for magnetic dipole (M_1) transitions between $I = \frac{1}{2}$ and $I = \frac{3}{2}$ nuclear spin manifolds are: $3 + 3\cos^2\theta$ ($\Delta M_I = +1$), $4\sin^2\theta$ ($\Delta M_I = 0$), $1 + \cos^2\theta$ ($\Delta M_I = -1$), $1 + \cos^2\theta$ ($\Delta M_I = +1$), $4\sin^2\theta$($\Delta M_I = 0$), $3 + 3\cos^2\theta$ ($\Delta M_I = -1$) where the foregoing correspond to a listing in order of increasing energy (velocity) (*8*). Thus, for $\theta = 0°$ ($\vec{E}_\gamma \| H_{Internal}$) the transition intensity ratio pattern is 3:0:1:1:0:3 while for $\theta = 90°$ the expected values are 3:4:1:1:4:3, again for thin, perfectly oriented absorbers. The intensity pattern for the right-hand side of Fig. 6 closely approximates the latter 1:4:3 ratio suggesting $\theta \sim 90°$. The weak absorption intensity (arrows in the centers of Figs. 5 and 6) is attributed to the sample impurity mentioned earlier and precludes

more exact comparisons. Under the usual assumption that the magnetization is coincident with H_{Internal}, one therefore concludes that *the electron spins and magnetization lie in the $FeClMoO_4$ sheets and are essentially normal to the c axis*. This result accords with the previous analysis of the combined quadrupole-Zeeman split spectra of the powder and neutron diffraction results to be discussed subsequently.

Spectra similar to that in Fig. 6 (bottom) for single crystals are generated for *powder samples* when determined in longitudinal applied fields ($H_0 \| \bar{E}_\gamma$). Figure 7 shows this effect as the progressive enhancement of the intensity of transitions 2 and 5 for H_o ranging from 0 to 4 T. We attribute this behavior to a relatively low field spin flop transition in the material, i.e., $H_{sf} \lesssim 1\ T$ (for instance, H_{sf} for single crystal α-Fe_2O_3 is 6.5 T at 4.2 K (*9*)). The application of even larger fields (up to 9 T) for both powder and single crystal mosaic samples caused little additional change in the shape of the spectrum from that shown at 4 T in Fig. 7. This is perhaps not surprising since the subsequent field-induced transition (in the H_o vs T phase diagram) for a uniaxial antiferromagnetic is the so-called spin-flop to "paramagnetic phase" transition that generally occurs at much larger values of H_o. The quantity H_{sf} is approximately equal to $(2H_AH_E)^{1/2}$ where H_A is the anisotropy field and H_E the exchange field. The high ordering temperature and implied high value for H_E and, at the same time, low value of H_{sf} are consistent with a relatively isotropic Fe^{3+} environment, its ^6A ground term, and small value for H_A.

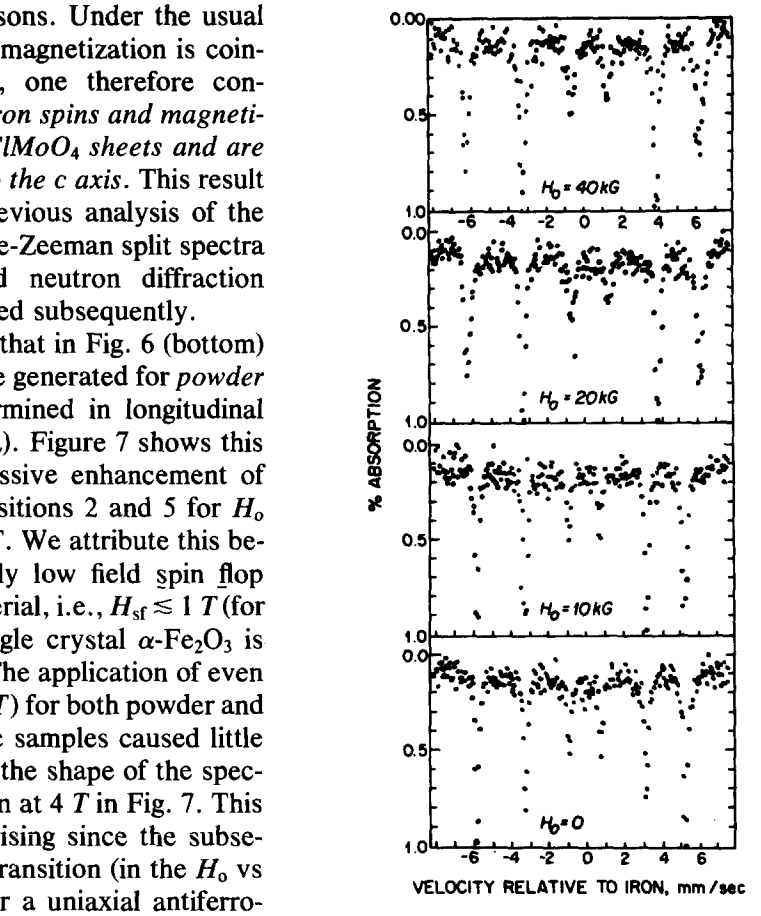

FIG. 7. Mössbauer spectra of $FeClMoO_4$ (powder) with $H_0 \| \bar{E}_\gamma$ and H_0 = 0 to 4 T showing the enhancement of the intensity of transitions 2 and 5 with increasing applied field.

3. Nuclear and Magnetic Structure

Profile fits and difference plots are shown in Fig. 8. Important interatomic distances for $FeClMoO_4$ at 4.85, 70, 181, and 300 K are given in Table IV. Iron–oxygen and molybdenum–oxygen distances of 1.95 and 1.76 Å, respectively, remain essentially constant from room temperature to 5 K. As the temperature decreases, the short Fe–Cl bond length within the FeO_4Cl square pyramid becomes elongated by 0.02 Å as the iron atom approaches the plane of the four basal oxygen atoms (Table IV). However, the long "nonbonded" interlayer iron–chlorine distance changes considerably. From 300 to 5 K, it decreases by 0.16 Å from 3.02 to 2.86 Å. Concurrent with the shortening of this Fe–Cl distance is a dramatic decrease in the tetragonal c-axis lattice parameter. A striking feature of the

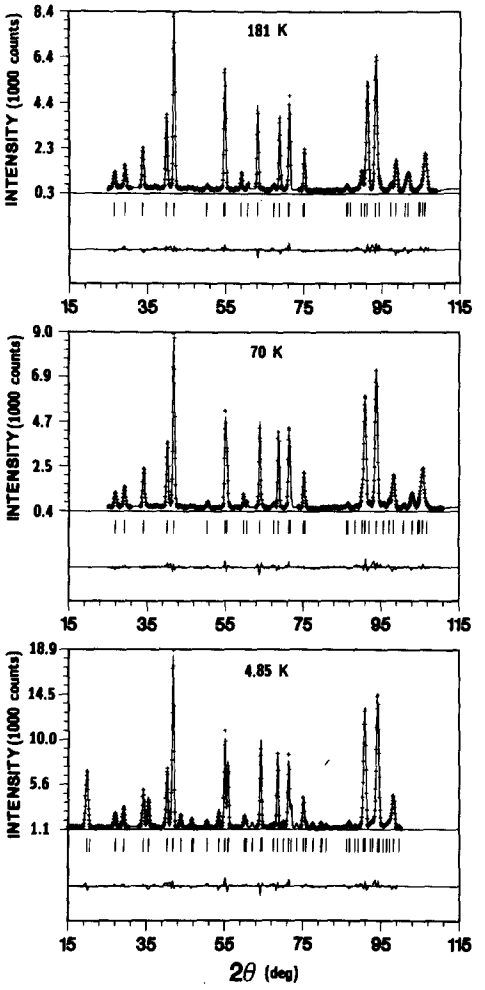

FIG. 8. Neutron powder diffraction profile fits and difference plots for $FeClMoO_4$ at 181, 70, and 4.8 K.

4.85 K data set is a shift of more than 2° in 2θ for several peaks with hkl; $l > 0$ when compared to the 181 K data. The a and c lattice parameters as a function of temperature are shown in Fig. 9. The c axis decreases by 2.7% from a value of 5.228 Å at 300 K to 5.089 Å at 4.85 K. Figure 9 shows the rate of change to be greatest in the vicinity of $T_N \simeq 70$ K, suggesting the occurrence of a magnetostrictive effect.

The maximum in the length of the a axis (Fig. 9) may be explained by a study of the

TABLE IV

IMPORTANT INTERATOMIC DISTANCES IN $FeClMoO_4$ AS A FUNCTION OF TEMPERATURE

	Intralayer distances (Å)			
	4.85 K	70 K	181 K	300 K[a]
Fe–Cl	2.232(4)	2.228(4)	2.210(4)	2.209(2)
Fe–Oa	1.960(2)	1.957(2)	1.952(2)	1.954(1)
Mo–Oa	1.759(2)	1.757(2)	1.759(2)	1.756(1)
Oa–Cl	3.205(4)	3.219(4)	3.223(5)	3.232(2)
Oa–Ob	2.734(3)	2.722(3)	2.706(3)	2.705(2)
Oa–Oc	2.819(4)	2.834(4)	2.841(5)	2.846(3)
Oa–Od	2.898(4)	2.886(4)	2.888(4)	2.877(3)
Fe–O_4[b]	0.32	0.35	0.38	0.40
	Interlayer distances (Å)			
Fe–Cl	2.857(4)	2.898(4)	2.981(4)	3.015(2)
Oa–Cl	3.186(4)	3.191(4)	3.227(5)	3.243(2)

[a] Single crystal X-ray results, Ref. (*1*).
[b] Distance between iron and the base of the FeO_4Cl square pyramid.

O–O and O–Cl distances in Table IV. As the layers approach one another, the four oxygen atoms of the FeO_4Cl square pyramids move away from each other in the

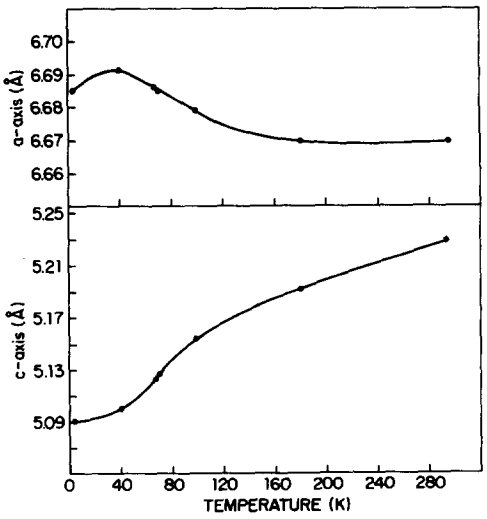

FIG. 9. Variation in the tetragonal lattice parameters of $FeClMoO_4$ as a function of temperature.

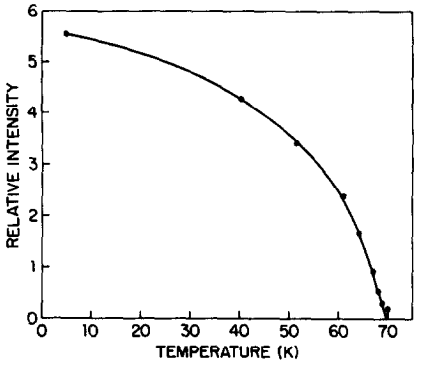

FIG. 10. Intensity of the $\frac{1}{2}\ \frac{1}{2}\ \frac{1}{2}$ magnetic peak of $FeClMoO_4$ as a function of temperature.

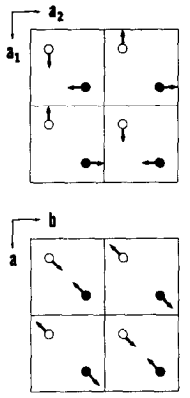

FIG. 11. Projection of the two possible magnetic cells for $FeClMoO_4$: (top) tetragonal, (bottom) orthorhombic.

(001) plane. Because the iron atom continuously moves closer to the plane of these O atoms, the Fe–O distance remains essentially constant over the 300 to 5 K range. Also, within the MoO_4 tetrahedra, the O–O separations that lie in the (001) plane remain constant to at least 70 K. This accounts for a basal expansion. Between 70 and 4.85 K, these molybdate O–O distances become shorter as the O–O distances of the FeO_4Cl square pyramids continue to get longer. A balance between these effects is reached at approximately 40 K and a maximum in the a axial length results. As expected, the O–Cl distances become shorter as the layers are drawn together with the interlayer O–Cl distances becoming shorter than the intralayer O–Cl distances.

From previous Mössbauer experiments, the temperature dependence of the internal hyperfine field indicated $T_N = 69.2 \pm 0.1$ K (*1*). This is in excellent agreement with the value of $T_N = 69$ K obtained from a plot of the intensity of the magnetic $(\frac{1}{2}\ \frac{1}{2}\ \frac{1}{2})$ peak as a function of temperature (Fig. 10). Other Mössbauer results, discussed above, indicate that magnetic ordering occurs with the moments oriented primarily within the $FeClMoO_4$ sheets. This is supported by the analysis of the magnetic peak intensities.

Figure 11 shows projections of the two *magnetic* cells (tetragonal and orthorhombic) viewed along the c axis, and illustrates the Fe atomic positions in eight structural cells (four cells above and four cells below). The arrows represent the magnetic moment directions within an $FeClMoO_4$ layer. Full and open circles represent iron atoms within a layer at $z_{mag} = z_{nuc}/2 = 0.27/2$ and $-z_{mag} = -z_{nuc}/2 = -0.27/2$, respectively. Iron atoms at $\frac{1}{2} + z_{mag}$ and $\frac{1}{2} - z_{mag}$ (i.e., an adjacent $FeClMoO_4$ layer) have their moments oriented in the opposite direction. It may be seen from the figure that an important feature of this structure is that moments on the $\frac{1}{4}\ \frac{1}{4}\ z$ sublattice have equal numbers of parallel and antiparallel neighbors on the $\bar{\frac{1}{4}}\ \bar{\frac{1}{4}}\ \bar{z}$ sublattice and hence the two sublattices can be only very weakly coupled.[2] Inspection of the magnetic structure reveals no obvious superexchange path analogous to that within a sublattice described below. The moment obtained from the refinement, 4.21(3) μ_B, is a little lower than usual (5.0 μ_B) and may be the

[2] This is similar to a number of other systems with lower dimensional properties, such as K_2NiF_4 and related compounds discussed in Ref. 1.

result of enhanced zero-point spin deviation characteristic of one- and two-dimensional magnetism (*10*).

4. Low-Dimensional Magnetism

Selection of a one-dimensional chain or two-dimensional layer model for the observed low dimensionality (*1*) is influenced by the interpretation of the structure and possible superexchange pathways. Thus, one possibility is that the material exhibits 1D antiferromagnetism via chains of corner-shared FeO_4Cl_2 octahedra linked through *trans* chlorine atoms extending along the tetragonal *c* direction. The iron atoms within the chains are shifted toward one chlorine atom and considerably away from the other chlorine atom such that "chains" contain alternating short and long Fe–Cl distances of 2.209(2) and 3.015(2) Å at room temperature ($d(Fe^{3+}–Fe^{3+})$ = 5.223 Å). The weaker "*interchain*" interactions leading to ultimate three-dimensional antiferromagnetic ordering presumably occur through angular O–Mo–O bridging units (O–Mo–O angle = 109.5°), and where each Fe^{3+} ion is connected to a tetragonal array of four near-neighbor Fe^{3+} ions ($Fe^{3+}–Fe^{3+}$ = 6.672 Å) via four such bridging MoO_4 tetrahedra. From the location of $T_{\chi max}$, one can estimate a value of $J_{intrachain}$ for a *Heisenberg chain* using the relation $k_B T_{\chi max}/|J|$ = 10.6 (*11*) and in the present case one obtains $|J|$ = 6.8 cm^{-1} (9.8 K). An alternate view leading to two-dimensional magnetic interactions is that the superexchange interactions are stronger in the $FeClMoO_4$ layers composed of four-coordinate $Mo(VI)O_4$ tetrahedra and five-coordinate FeO_4Cl square pyramids. The Mo(VI) corresponds to diamagnetic d^0 and contributes nothing to the paramagnetism of the system. Three-dimensional ordering at ~69 K is then the result of weak *interlayer* exchange probably via the long "nonbonded" Fe–Cl distance (3.015 Å). As in the preceding case of a chain, one can estimate the intralayer exchange simply from $T_{\chi max}$. For a quadratic Heisenberg magnet, the relationship is $k_B T_{\chi max}/|J|S(S+1)$ = 2.05 (*11*) which leads to $|J|$ = 4.0 cm^{-1} (5.8 K) in the present case.

Generally, linear bridging units (*M–X–M* angle ~180°) constitute stronger antiferromagnetic exchange pathways than those that are near orthogonal. In addition, the fewer the number of bridging formally diamagnetic atoms in the superexchange unit, the stronger the exchange interaction (save for unusual conjugation effects in unsaturated organo-bridging units). In our first communication (*1*) on $Fe(III)ClMoO_4$, a two-dimensional interpretation of the low dimensionality was favored, primarily on the basis of the fact that the 1D chain exchange pathway involves long (~3.0 Å) essentially "nonbonded" segments alternating with genuine Fe(III)–Cl bonds (~2.2 Å). Although the metal–metal separations are longer and nonlinear within the layers, the interactions between the Fe^{3+} ions are truly bonded and there are twice as many such bridging units per iron atom. In retrospect, it is simply not clear that the latter *2D view* of the low dimensionality of $Fe(III)ClMoO_4$ is correct. Detailed fits of the temperature dependence of the average *powder* susceptibility data to various approximate high-temperature series expansion models (*11*) of 1D and 2D behavior does *not allow* for unequivocable distinction and preference for a 1D over a 2D view of the low dimensionality, especially when the real spin of the system is so large, $S = \frac{5}{2}$. The difference in the $|J|$ for two reasonable models for a ^6A ground state ion (Heisenberg chain vs quadratic Heisenberg layer) based on the position of $T_{\chi max}$ is only ~3 cm^{-1}. In order to clarify this situation, a study of the diffuse magnetic scattering above T_N by single crystal neutron diffraction would be necessary.

Acknowledgments

W. M. R. is pleased to acknowledge the continued support of the National Science Foundation Division of Materials Research, Solid State Chemistry Program Grant DMR 8313710. He also wishes to express his thanks for time on the SQUID magnetometer facility at the Francis Bitter National Magnet Laboratory-MIT. Work performed at Brookhaven is supported by the Division of Materials Science U.S. Department of Energy under Contract DE-AC02-76CH00016.

References

1. C. C. TORARDI, J. C. CALABRESE, K. LÁZÁR, AND W. M. REIFF, *J. Solid State Chem.* **51,** 376 (1984).
2. C. CHENG AND W. M. REIFF, *Inorg. Chem.* **16,** 2097 (1977).
3. H. M. RIETVELD, *J. Appl. Crystallogr.* **2,** 65 (1969).
4. L. KOESTER, *in* "Neutron Physics", Springer Tracts in Modern Physics, Vol. 80, pp. 1–55, Springer Verlag, Berlin (1977).
5. R. E. WATSON AND A. J. FREEMAN, *Acta Crystallogr.* **14,** 27 (1961).
6. W. OPECHOWSKI AND R. GUCCIONE, *in* "Magnetism" (G. T. Rado and H. Suhl, Eds.), Vol. IIA, p. 105, Academic Press, New York (1965).
7. C. KITTEL, "Introduction to Solid State Physics," 5th ed., pp. 482–483, Wiley, New York (1976).
8. N. N. GREENWOOD AND T. C. GIBB, "Mössbauer Spectroscopy," Chapman & Hall, London (1971).
9. W. M. REIFF, *Coord. Chem. Rev.* **10,** 37 (1972).
10. G. P. GUPTA, D. P. E. DICKSON, AND C. E. JOHNSON, *J. Phys. C* **13,** 2071 (1980).
11. L. J. DE JONGH AND A. R. MIEDEMA, *Adv. Phys.* **23,** 1 (1974).